

# Removing grid structure in angle-resolved photoemission spectra via deep learning method

Junde Liu,<sup>1,2,\*</sup> Dongchen Huang,<sup>1,2,\*</sup> Yi-feng Yang,<sup>1,2,3,†</sup> and Tian Qian<sup>1,2,3,‡</sup>

<sup>1</sup>*Beijing National Laboratory for Condensed Matter Physics and Institute of Physics, Chinese Academy of Sciences, Beijing 100190, China*

<sup>2</sup>*University of Chinese Academy of Sciences, Beijing 100049, China*

<sup>3</sup>*Songshan Lake Materials Laboratory, Dongguan, Guangdong 523808, China*

(Dated: October 21, 2022)

Spectroscopic data may often contain unwanted extrinsic signals. For example, in ARPES experiment, a wire mesh is typically placed in front of the CCD to block stray photo-electrons, but could cause a grid-like structure in the spectra during quick measurement mode. In the past, this structure was often removed using the mathematical Fourier filtering method by erasing the periodic structure. However, this method may lead to information loss and vacancies in the spectra because the grid structure is not strictly linearly superimposed. Here, we propose a deep learning method to effectively overcome this problem. Our method takes advantage of the self-correlation information within the spectra themselves and can greatly optimize the quality of the spectra while removing the grid structure and noise simultaneously. It has the potential to be extended to all spectroscopic measurements to eliminate other extrinsic signals and enhance the spectral quality based on the self-correlation of the spectra solely.

## I. INTRODUCTION

In the past decades, ARPES has driven the research of novel quantum materials with its incredible ability to directly probe the electronic structures [1–7]. Owing to the rapid development of experimental techniques, highly rapid data acquisition modes (“Fixed” or “Dithered” modes) are frequently required in many application scenarios. For example, the fast scanning mode is often used in spatial-resolved ARPES experiments to map the energy band spectra of a wide area of the sample [8, 9]. It is also preferred when the spot size of the laser beam is tiny, in which case the measurement should be limited to a very short time to avoid sample damage [10]. In addition, the fast scanning mode can save a lot of acquisition time for measuring higher-dimensional data, such as band structures in two-dimensional momentum space or dynamical electronic structures in time-resolved ARPES [11–15].

However, because of the metal mesh in front of the analyzer CCD, the spectra obtained using the fast scanning mode typically have a grid-like structure as shown in Fig. 1(a) [7, 16], which hinders the direct observation of energy band features. Although the grid structure may be averaged out using the swept mode, measurements in this mode often cover a large portion of unwanted energy ranges, causing a great time waste in opposition to the original purpose. Post-spectral processing techniques and methods are hence needed to remove this grid structure.

A traditional method is to use Fourier filtering by con-

verting the real space spectra to the Fourier domain [16]. But simply erasing the peaks in Fourier space may lose intrinsic information because the grid structure is not strictly periodic and linearly superimposed. For instance, the peaks and energy bands in Fourier space may merge together when their widths are comparable, which makes it difficult to remove the peaks without losing information about the energy bands. It may become even more challenging when the data quality is noisy or not good enough so that the peaks in Fourier space cannot be well identified. Therefore, the traditional Fourier filtering method requires the peaks in Fourier space to be sharp and distinguishable from the intrinsic bands, which essentially limits the range of its application scenarios.

Fortunately, machine learning methods have shown strong capabilities in spectra processing [17–20]. Deep learning-based methods can achieve better performance than traditional mathematical Gaussian smoothing methods in removing noise from spectra [20]. More surprisingly, we have shown that a noisy spectra image can be decomposed into an image of clean spectra and an image corresponding to noise, provided that the noise is sparse and not so coherent with the intrinsic energy bands. This inspired us to view the grid structure as an extrinsic signal, so that the spectra may be decomposed into a clean part and a grid part.

Following the above line of thought, we propose in this work a deep learning-based method to remove the grid structure and identify the intrinsic signal in the measured ARPES spectra. Our method utilizes the self-correlation information of the spectra themselves and parameterizes the observed ARPES data by two convolutional neural networks (CNNs). One network is designed to extract the clean spectra, and the other aims to extract the grid texture. We show that this enables us to preserve the signal of the energy bands in the spectra even if the grid width and energy bandwidth are comparable or the spec-

\*These authors contributed equally to this work.

†yifeng@iphy.ac.cn

‡tqian@iphy.ac.cn

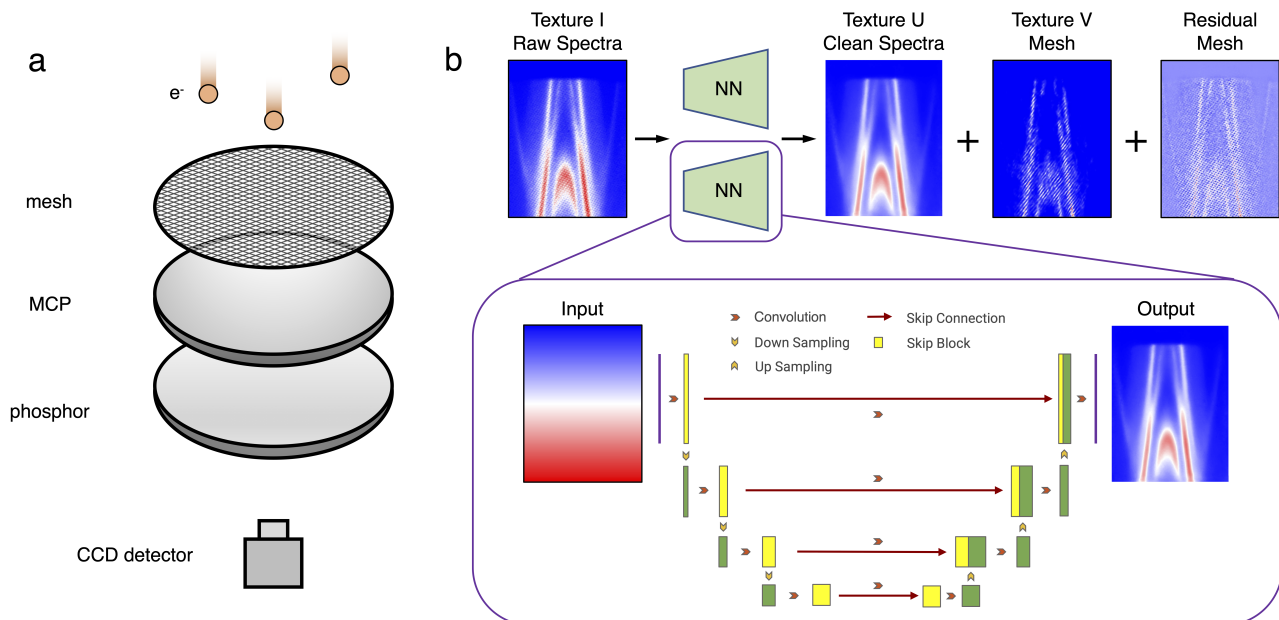


FIG. 1: (a) An illustration of the ARPES analyzer. (b) The raw spectra image are parameterized as a mixture of two textures. The first texture aims to recover the spectra and the other finds the grid structure somewhat attached to the energy bands. The residual is the general grid structure, since the neural network does not learn all the features in the input image.

tral quality is not so good. As a result, our method can nicely remove the grid structure and extend the application of the fast scanning mode, which is essential for ARPES experiments. Our idea can be applied to any extrinsic structures from other multidimensional data, thus improving the quality of the spectra obtained in more general scenarios.

## II. METHODS

We start by assuming that a complex image can be represented by a mixture of two or more simple components or textures, each of which can be viewed as an image. At first glance, this seems impossible and under-determined because the unknown parameters are more than the known ones. But this problem has been proved solvable in high-dimensional analysis if one component is incoherent with another [21, 22]. In other words, pixels or patches are correlated within each texture but independent of those within another texture. This insight has led to successful algorithms showing reasonable performance in computer vision [23, 24] and ARPES de-noising [25] even without requiring a training set.

Motivated by these successes, we extend the above idea and develop an algorithm for de-gridding the ARPES data. As shown in Fig. 1(b), we attempt to decompose a raw spectra image  $I$  into two textures  $U$  and  $V$  and expect that  $U$  gives the clean spectra and  $V$  approximates the grid structure. All the images  $I, U, V$  may be viewed as matrices, and the entries in  $U$  or  $V$  should be correlated. We parameterize each texture via a U-shape

neural network [26], which has shown good performance in modelling correlated data and real-world tasks in computer vision [26].

The summation of both textures  $U, V$  should give the raw spectra  $I$ , which we take as the loss function. This yields

$$\min_{\theta, \phi} \|I - U_{\theta} - V_{\phi}\|_F^2, \quad (1)$$

where  $\theta, \phi$  are the parameter collections for each neural network, and  $\|\cdot\|_F^2$  denotes the square of the Frobenius norm, which is defined as the summation of all entries of a matrix. The parameters are then optimized by stochastic gradient descent (SGD) with respect to the loss function given in eq. (1). Our algorithm is implemented via Pytorch [27] and the detailed training hyperparameters are listed in Appendix B.

*a. Noisy data.* In practice, noise is unavoidable in the raw data. To make the algorithm more practical, we combine de-noising techniques into this framework. The noise  $s$  is assumed to be sparse because an image of measured spectra should not be corrupted everywhere. Following similar techniques [28], we decompose the raw spectra into three textures: the clean spectra  $U$ , the grid structure  $V$ , and the noise  $s$ . As discussed in [25], the noise can be further parameterized as  $s = a \circ a - b \circ b$ , where  $a, b$  are two vectors with learnable entries, and the symbol  $\circ$  denotes their element-wise product. The loss function now becomes

$$\min_{\theta, \phi, a, b} \|I - U_{\theta} - V_{\phi} - a \circ a + b \circ b\|_2^2, \quad (2)$$

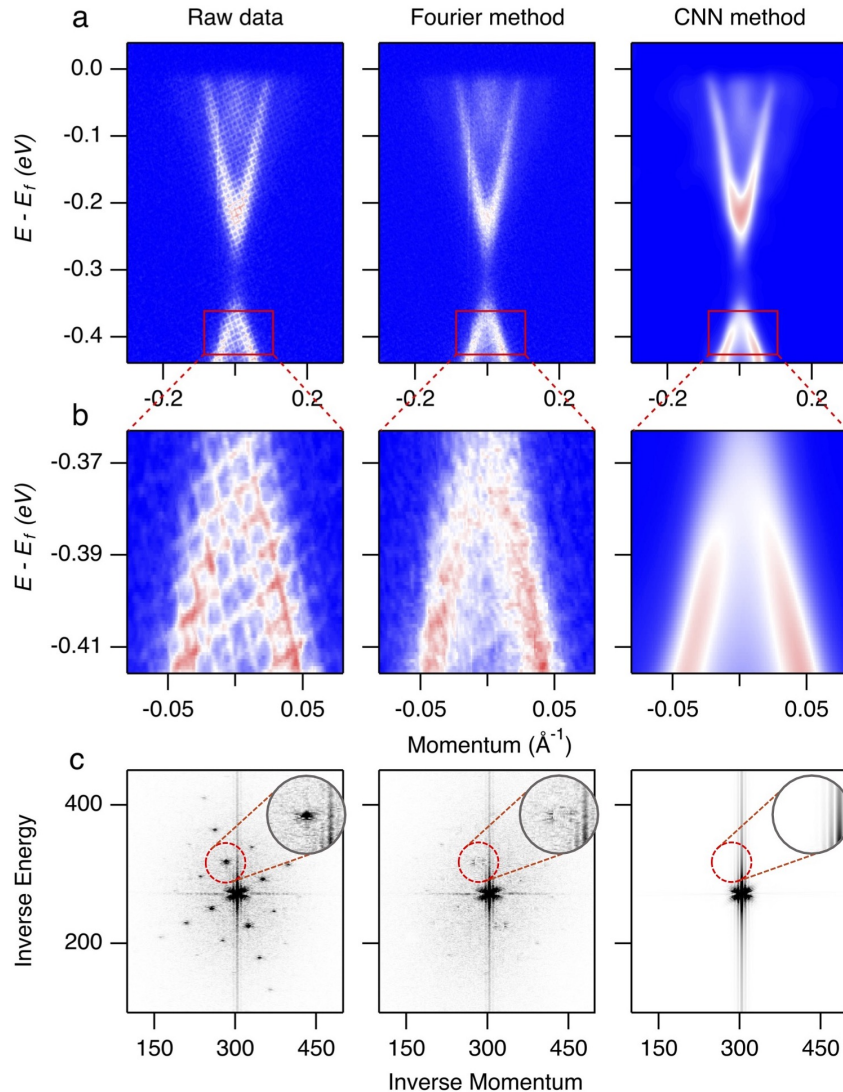


FIG. 2: Comparison of the de-gridded results using different methods. (a)  $\text{MnBi}_2\text{Te}_4$  ARPES data along the cut through  $\bar{\Gamma}$  and the de-gridded results based on the Fourier filtering method and our deep-learning method. (b) Close-up showing of the area in the red box region indicated in panel (a). (c) Corresponding Fourier transform results of panel (a). The inset shows the close-up of the first-order peak and energy band signals indicated with red circle.

where every matrix is flattened as a vector and  $\|\cdot\|_2^2$  denotes the square of  $\ell^2$  norm. We find quite stable training with the form in eq. (2).

### III. APPLICATIONS

Fig. 2(a) shows the raw data and the de-gridded results using different methods for ARPES data of  $\text{MnBi}_2\text{Te}_4$  along the cut through  $\bar{\Gamma}$ . The raw data were measured in the fast scanning mode. The quasi-periodic grid structure is clearly visible in the raw data, as may be best viewed in the enlarged plot Fig. 2(b). The grid structures overlap with the energy band features, which may hinder the observation and analysis of some fine details.

Fig. 2(c) shows the spectra in the Fourier space after applying the Fourier transform to the data in Fig. 2(a). We see that the energy band signals are concentrated in the central region and along the lines due to its non-periodic nature, while the signals of the quasi-periodic grid structure yields the Fourier peaks distributed symmetrically near the diagonals of the image, whose locations represent the reciprocal vectors of the grid. The inset (red circle) shows the close-up of the first-order Fourier peak and energy band signals. They are quite close to each other, making it extremely difficult to erase the grid structure without losing intrinsic information.

The de-gridded results by using the Fourier filter-based method and the deep learning-based method are compared in Fig. 2(b). While both methods can remove

the grid structure from the original spectra, the quality of the resulting spectra processed by the deep learning-based method is obviously much better. We see that the deep learning-based spectra are very clean and smooth, but the Fourier filter-based ones are still rough and even contain some empty spaces. This is because the existence of the grid structure interferes with the acquisition of the intrinsic energy band signals in the measurement process. As a result, simply erasing the Fourier peaks fails to fill the missing intrinsic signal affected by the grid structure and thus loses the corresponding energy band features. Indeed, as shown in Fig. 2(c), it is difficult for the Fourier filter-based method to completely remove the Fourier peaks without affecting the intrinsic energy band signal. By contrast, deep learning-based methods can naturally and directly extract the complete intrinsic energy band signal through local correlation without losing critical information. It not only eliminates the Fourier peaks entirely but also completes the intrinsic energy band signal, making the spectra quite smooth and comprehensive. More examples can be found in Appendix A.

## IV. DISCUSSION

### A. The training dynamics

As described above, the deep learning-based method can remove the weak-correlated extrinsic grid structure and extract the local strong-correlated intrinsic energy band signals. The reason of its good performance may be ascribed to the correlation of neighboring pixel values in the spectra of ARPES experiments. The regions of energy band features generally span a finite range and contain a number of pixel points whose intensity does not exhibit large fluctuations. Contrarily, changes brought by the grid structure are more localized, and their correlation is much weaker. Therefore, even if the grid has contaminated the information at a pixel, the value at that pixel can be retrieved by inferring the most statistically probable value from nearby pixel values while retaining the intrinsic information from the energy band.

To demonstrate how the algorithm extracts the intrinsic energy band signal, we present the dynamical processing results of  $\text{Ir}_{1-x}\text{Pt}_x\text{Te}_2$  ARPES data in Fig. 3. It can be seen that as the iteration of the computing process increases, the intrinsic energy band signals are gradually extracted [Fig. 3(a)], leaving only the grid structure [Fig. 3(b)]. Specifically, at zero iteration, the extracted signal is the random initial input. As the number of iterations increases to 25, the contours of the two energy bands start to emerge. Although the band structures are very crude at this stage, they have already covered all the area where the real energy bands are located. As the iteration increases to 100 and 400, more detailed structures are revealed and we eventually obtain the clear spectra. The computing process tends to extract the signals [Fig.

3(a)] with more local and stronger correlations from the remaining spectra [Fig. 3(b)] to produce the intrinsic band structures.

Fig. 3(c) plots the evolution of the loss function  $L(x, f(x'))$  with the training iteration. We see that it decreases rapidly from the initial point to iteration 25. As shown in Fig. 3(a), the algorithm first captures the general shape of the energy bands, indicating that the weak global correlations can be extracted quite easily. As the correlation information in the energy bands to be extracted becomes stronger and more local, the loss decreases more slowly. After approximately 300 iterations, the loss converges to a small value. The convergence shows that the algorithm can no longer extract more local correlation information and the model is not overfitted to the grid structure, thus ensuring that the energy band information of the intrinsic signals may be largely preserved. From this point of view, we may conclude that the neural network first learns low-frequency long-range features and then adds high-frequency local details during the training.

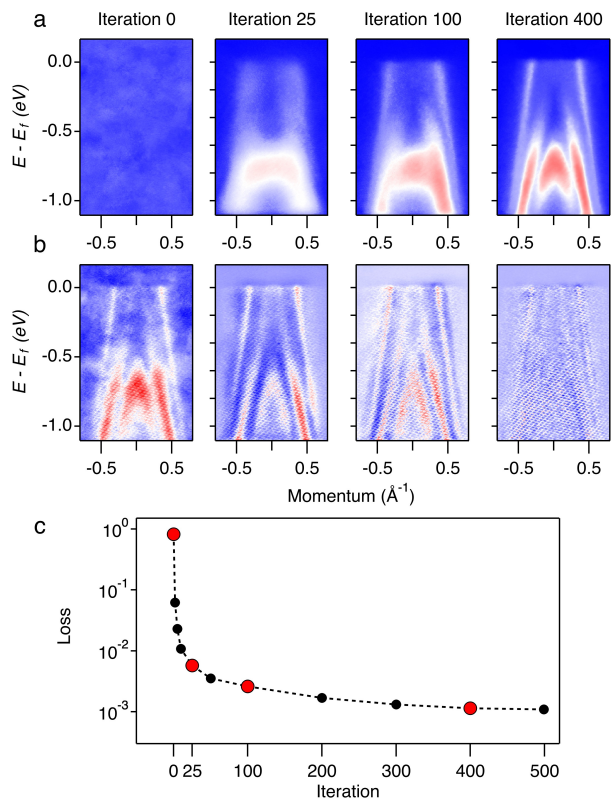


FIG. 3: Intermediate results during the training process depending on iteration. (a)  $\text{Ir}_{1-x}\text{Pt}_x\text{Te}_2$  ARPES data and iteration-dependent de-gridded results for the iteration steps 0, 25, 100, and 400, which denotes the number of loops in the computing process. (b) Corresponding residual spectra of (a). (c) Loss  $L(x, f(x'))$  as a function of the iteration. The corresponding iteration numbers plotted in (a) and (b) are highlighted with enlarged red circles.

## B. Effect of de-noising

As the grid structure is removed, the spurious noise is also seen to be removed from the spectra and the quality of the resulting spectra is greatly improved. To quantitatively evaluate the performance of de-noising, we use line shape analysis on  $\text{Ir}_{1-x}\text{Pt}_x\text{Te}_2$  ARPES data. As shown in Fig. 4(a), our method can preserve the intrinsic band structures while removing the noise compared to the original data and the de-gridded results using the Fourier filtering method. This is more clearly seen in the smoother momentum distribution curves (MDCs) shown in Fig. 4(b) and Fig. 4(c) for the area indicated by the white box region in Fig. 4(a).

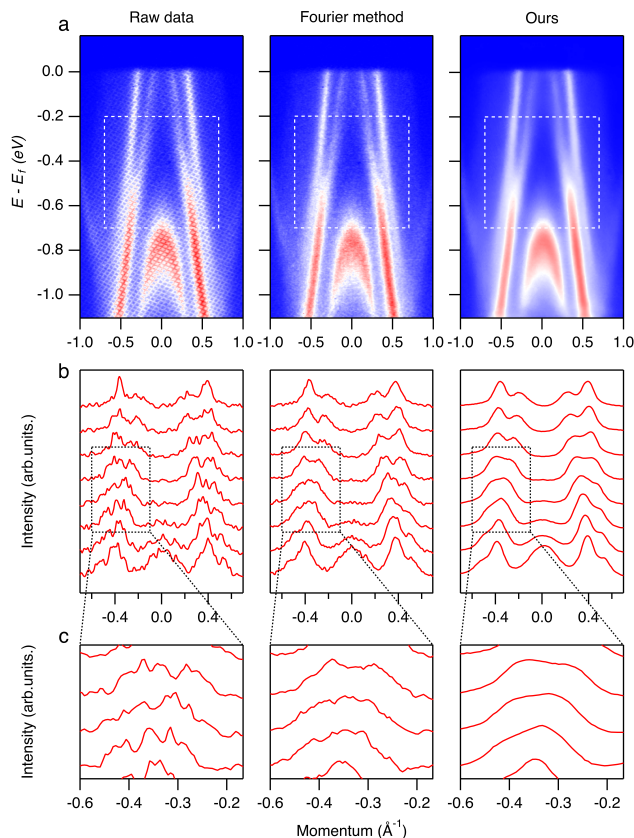


FIG. 4: Comparison analysis of different methods. (a) The raw data of ARPES spectra for  $\text{Ir}_{1-x}\text{Pt}_x\text{Te}_2$  and the de-gridded results based on the Fourier filtering method and the deep-learning method. (b) Corresponding momentum distribution curves (MDCs) of the area in the white box region indicated in panel (a). (c) Close-up showing of the area in the black box region indicated in panel (b).

The reason why the noise can be simultaneously removed should be attributed to the foundation of our method, which respects the locally correlated intrinsic energy bands in noisy and grid-like spectra. It has been proved [21] that if a signal is a superposition of some incoherent components, each component can be identi-

fied by proper parameterization and optimization. In the analysis of spectroscopic measurements, both the spurious noise signals and grid structures are weakly correlated with the intrinsic energy bands. Their superposition, combined with the intrinsic energy bands, gives the raw spectra. We may hence view them as three nearly independent parts. Thus, by parameterizing them via three corresponding neural networks in eq. (2), we can separate them from the total spectra and identify the intrinsic energy bands as shown in Fig. 4(a). This setting is easily generalisable, so our method can be extended to many application scenarios to remove different extrinsic signals simultaneously and achieve clear and desired spectra.

## V. CONCLUSION

In this work, we propose a deep-learning-based method to eliminate the grid-like structure in fast scanning mode for ARPES spectroscopy. This is quite helpful for saving measurement time and enhancing the spectral quality. Compared to the traditional Fourier filtering methods, our deep learning method can extract the intrinsic information directly by making use of the local correlation nature of the energy band signals. It can remove extrinsic features including the grid structure and noise simultaneously, and thus greatly improve the spectra. Our algorithm may also be extended to other spectroscopic measurements for removing unwanted signals, including quasi-periodic structures, spurious signals, noise, etc.

## ACKNOWLEDGEMENTS

We thank Mojun Pan, Famin Chen, Jierui Huang, and Bei Jiang for useful discussions, and Zhicheng Rao, Shunye Gao, and Wenhui Fan for data support. This work was supported by the National Natural Science Foundation of China (NSFC Grants Nos. U1832202, 11888101, 11974397, 12174429), the Chinese Academy of Sciences (Grant Nos. QYZDB-SSW-SLH043, XDB33000000, and XDB28000000), the Informatization Plan of Chinese Academy of Sciences (Grant No. CAS-WX2021SF-0102), and the Synergetic Extreme Condition User Facility (SECUF).

## APPENDIX A: MORE EXAMPLES

Fig. 5 shows more de-gridded examples based on the deep-learning method. Regardless of sharp or diffuse energy bands in the spectra, our method can always remove the grid structure and extract well the intrinsic energy band information. This indicates that our method based on CNNs is quite stable and has a strong potential for generalization.

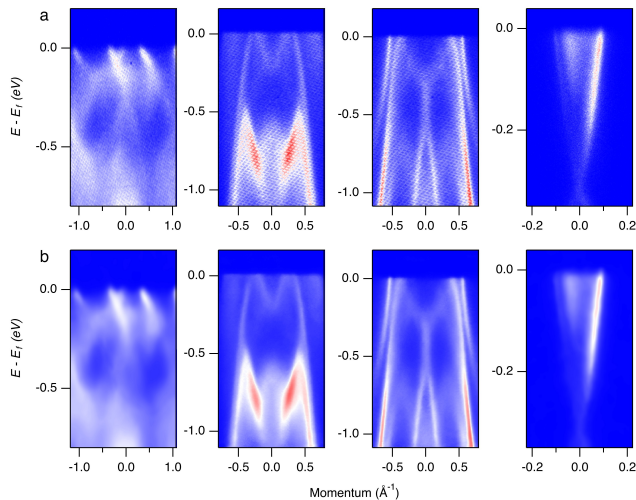


FIG. 5: The de-gridded results for more ARPES spectra. (a) The raw data with grid-like structure; (b) The corresponding de-gridded results based on our deep-learning method.

## APPENDIX B: IMPLEMENTATION DETAILS

The neural network parameters are listed in Table I. We use batch normalization (BN) [29] every layer, and set the parameter of leaky-ReLU to 0.2. This algorithm

is not sensitive to the input, so we use similar inputs as reported in previous work [23, 28], plus a small fraction ( $\sim 0.01$ ) of the raw data in this work. To achieve better results, discrepant learning rates should be used for the three neural networks. We find (0.2, 2, 600) is an appropriate parameter choice for many ARPES images.

TABLE I: Neural network architecture

Encoder network	
Input spectra $x$	
Conv2d, BN, $5 \times 5 \times 16$ , stride=2, lReLU	
Conv2d, BN, $5 \times 5 \times 32$ , stride=2, lReLU	
Conv2d, BN, $5 \times 5 \times 64$ , stride=2, lReLU	
Conv2d, BN, $5 \times 5 \times 128$ , stride=2, lReLU	
Conv2d, BN, $5 \times 5 \times 128$ , stride=2, lReLU	
Decoder network	
Conv2d, BN, $5 \times 5 \times 128$ , stride=1, lReLU	
Upsampling, Conv2d, BN, $5 \times 5 \times 128$ , stride=1, lReLU	
Upsampling, Conv2d, BN, $5 \times 5 \times 64$ , stride=1, lReLU	
Upsampling, Conv2d, BN, $5 \times 5 \times 32$ , stride=1, lReLU	
Upsampling, Conv2d, BN, $5 \times 5 \times 16$ , stride=1, lReLU	
Conv2d, $1 \times 1 \times 1$ , stride=1, sigmoid	

- [1] A. Damascelli, Z. Hussain, and Z.-X. Shen, *Rev. Mod. Phys.* **75**, 473 (2003).
- [2] M. Hashimoto, I. M. Vishik, R.-H. He, T. P. Devereaux, and Z.-X. Shen, *Nat Phys.* **10**, 483 (2014).
- [3] H. Yang, A. Liang, C. Chen, C. Zhang, N. B. M. Schroeter, and Y. Chen, *Nat Rev Mater.* **3**, 341 (2018).
- [4] C. Zhang, Y. Li, D. Pei, Z. Liu, and Y. Chen, *Annu Rev Mater Res.* **50**, 131 (2020).
- [5] B. Lv, T. Qian, and H. Ding, *Nat Rev Phys.* **1**, 609 (2019).
- [6] B. Q. Lv, T. Qian, and H. Ding, *Rev. Mod. Phys.* **93**, 025002 (2021).
- [7] J. A. Sobota, Y. He, and Z.-X. Shen, *Rev. Mod. Phys.* **93**, 025006 (2021).
- [8] I. Hideaki, S. F. Eike, A. Masashi, I. Akihiro, N. Hirofumi, T. Masaki, A. Yoshihiro, and S. Kenya, *Ultramicroscopy.* **182**, 85 (2017).
- [9] M. Cattelan and N. A. Fox, *Nanomaterials.* **8**, (2018).
- [10] M. E. Grass, P. G. Karlsson, F. Aksoy, M. Lundqvist, B. Wannberg, B. S. Mun, Z. Hussain, and Z. Liu, *Rev Sci Instrum.* **81**, 053106 (2010).
- [11] J. Orenstein, *Phys Today.* **65**, 44 (2012).
- [12] H. Aoki, N. Tsuji, M. Eckstein, M. Kollar, T. Oka, and P. Werner, *Rev Mod Phys.* **86**, 779 (2014).
- [13] C. L. Smallwood, R. A. Kaindl, and A. Lanzara, *Epl-Europhys Lett.* **115**, 27001 (2016).
- [14] C. Bao, P. Tang, D. Sun, and S. Zhou, *Nat Rev Phys.* **4**, 33 (2022).
- [15] A. de la Torre, D. M. Kennes, M. Claassen, S. Gerber, J. W. McIver, and M. A. Sentef, *Rev Mod Phys.* **93**, 041002 (2021).
- [16] S. Liu, E. Kotta, Y. Xu, J. Mutch, J.-H. Chu, M. Hoesch, S. K. Mahatha, J. D. Denlinger, and L. A. Wray, arXiv: 2112.11516 (2021).
- [17] P. Zhang, P. Richard, T. Qian, Y.-M. Xu, X. Dai, and H. Ding, *Rev Sci Instrum.* **82**, 043712 (2011).
- [18] Y. He, Y. Wang, and Z.-X. Shen, *Rev Sci Instrum.* **88**, 073903 (2017).
- [19] H. Peng, X. Gao, Y. He, Y. Li, Y. Ji, C. Liu, S. A. Ekahana, D. Pei, Z. Liu, Z. Shen, and Y. Chen, *Rev Sci Instrum.* **91**, 033905 (2020).
- [20] Y. Kim, D. Oh, S. Huh, D. Song, S. Jeong, J. Kwon, M. Kim, D. Kim, H. Ryu, J. Jung, W. Kyung, B. Sohn, S. Lee, J. Hyun, Y. Lee, Y. Kim, and C. Kim, *Rev Sci Instrum.* **92**, 073901 (2021).
- [21] E.J. Candès, X. Li, Y. Ma, and J. Wright, *J Acm Jacm.* **58**, 11 (2011).
- [22] J. Wright and Y. Ma, *IEEE T Inform Theory.* **56**, 3540 (2010).
- [23] D. Ulyanov, A. Vedaldi, and V. Lempitsky, *Int J Comput Vision.* **128**, 1867 (2020).
- [24] Y. Gandelsman, A. Shocher, and M. Irani, in *Proceedings of the IEEE/CVF Conference on Computer Vision and Pattern Recognition (IEEE, Los Alamitos, 2019)*, pp. 11026-11035.
- [25] D. Huang, J. Liu, T. Qian, and Y.-F. Yang, arXiv: 2210.10494 (2022).
- [26] O. Ronneberger, P. Fischer, and T. Brox, in *Medical*

- Image Computing and Computer-Assisted Intervention – MICCAI 2015, edited by Nassir Navab, Joachim Hornegger, William M. Wells, and Alejandro F. Frangi (Springer International Publishing, Cham, 2015), pp. 234-241.
- [27] A. Paszke, S. Gross, F. Massa, A. Lerer, J. Bradbury, G. Chanan, T. Killeen, Z. Lin, N. Gimeshein, L. Antiga, A. Desmaison, A. Kopf, E. Yang, Z. DeVito, M. Raison, A. Tejani, S. Chilamkurthy, B. Steiner, L. Fang, J. Bai, and S. Chintala, in *Advances in Neural Information Processing Systems*, edited by H. Wallach, H. Larochelle, A. Beygelzimer, F. d’Alché-Buc, E. Fox and R. Garnett (Curran Associates, Inc., San Francisco, 2019)
- [28] C. You, Z. Zhu, Q. Qu, and Y. Ma, in *Advances in Neural Information Processing Systems*, edited by H. Larochelle, M. Ranzato, R. Hadsell, M.F. Balcan, and H. Lin (Curran Associates, Inc., San Francisco, 2020), pp. 17733-17744.
- [29] S. Ioffe and C. Szegedy, in *Proceedings of the 32nd International Conference on Machine Learning*, edited by Francis Bach and David Blei (PMLR, Lille, 2015), pp. 448-456.